Springer

Journal of Mechanical Science and Technology 22 (2008) 2337~2349

Journal of Mechanical Science and Technology

www.springerlink.com/content/1738-494x
DOI 10.1007/s12206-008-0915-6

Contact stress of O-ring under uniform squeeze rate by photoelastic experimental hybrid method †

Jeonghwan Nam [1], Jaisug Hawong[1,*], Songling Han[2] and Sunghan Park[3]

[1]*School of mechanical Engineering, Yeungnam University, Gyeongsan, 712-749, Korea*
[2]*Gradute School, School of mechanical Engineering, Yeungnam University, Gyeongsan, 712-749, Korea*
[3]*Agency for Defense Development, Daejeon, Korea*

(Manuscript Received January 25, 2008; Revised September 12, 2008; Accepted September 16, 2008)

Abstract

In this paper, photoelastic experimental hybrid methods using the external traction free boundary condition and that using the relative equation of two stress functions in contact problems are developed. The validities of these two methods are confirmed through experiments and discussions. Hertz's contact theory and the two photoelastic experimental hybrid methods explained are applied to the analysis of the contact stress of an O-ring under 10% or 20% squeeze rate. The photoelastic experimental hybrid method using the relative equation of two stress functions in contact problems was found to be more effective. When the squeeze rates of an O-ring were 10% or 20%, the maximum of absolute σ_x was greater than the maximum of absolute σ_y, but was almost equal. Maximums of absolute τ_{xy} were $1/8$ of absolute σ_x and $1/5$ of absolute σ_x when the squeeze rates of the O-ring were 10% and 20%, respectively.

Keywords: Contact problem; Hertz's contact theory; O-ring; Photoelastic experimental hybrid method; Squeeze rate; Stress Function; Stress freezing method; Internal stress

1. Introduction

Rubber O-rings have been used as packing elements for high pressure vessels, oil-pressure parts, air-plane parts and nuclear generator parts etc.

The design criterion of an O-ring can be determined by stress analysis for various loading conditions, which are dependent on the internal pressure and the fitting conditions of the O-ring. Stresses of the O-ring have been studied extensively by many researchers [1-5].

In this research, the photoelastic experimental hybrid method is applied to the stress analysis of the O-ring under uniform squeeze rate.

The hybrid technique has been studied by researchers [6, 7].

The photoelastic experimental hybrid method for determining the stress concentration factors and stress intensity factors of orthotropic materials under uniform tension[8, 9] and for determining the stress concentration factors and stress intensity factors of isotropic material under uniform tension [10, 11] were developed by the authors.

The dynamic photoelastic experimental hybrid method for isotropic materials, orthotropic materials, and biomaterials with cracks under dynamic loads was also developed by the authors [12-14].

In the photoelastic experimental hybrid method that has been used, the relationships with two stress functions obtained from the internal traction free boundary conditions such as a circular hole and crack were used.

Many structures used in various industrial fields have external traction free boundary conditions. Therefore, it is necessary to develop a photoelastic experimental hybrid method for structures with the external traction free condition. This study aims to

† This paper was recommended for publication in revised form by Associate Editor Joo Ho Choi

*Corresponding author. Tel.: +82 53 810 2445, Fax.: +82 53 813 4627
E-mail address: jshawong@yu.ac.kr

establish analysis procedures of contract stress and internal stress of the O-ring under a uniform squeeze rate as follows:

(1) To develop the photoelastic experimental hybrid method for structures with external traction free boundary condition

(2) To develop the photoelastic experimental hybrid method using the relative equation of two stress functions for a contact problem of the O-ring under a uniform squeeze rate

(3) Stress analysis of O-ring under uniform squeeze rates of 10% and 20% by the photoelastic experimental hybrid methods and the Hertz's contact theory

2. Basic Theory

2.1 Hertz's contact theory

Stress components are obtained by using the Muskhelishvili complex function [15] and Airy stress function as follows in Eq. (1).

$$\begin{aligned}\sigma_x &= \mathrm{Re}\left[2\phi'(z) - \bar{z}\phi''(z) - \Psi'(z)\right]\\ \sigma_y &= \mathrm{Re}\left[2\phi'(z) + \bar{z}\phi''(z) + \Psi'(z)\right]\\ \tau_{xy} &= \mathrm{Im}\left[\bar{z}\phi''(z) + \Psi'(z)\right]\end{aligned} \tag{1}$$

Where, $z = x + iy$

Re(Im): real(imaginary) part of complex.

As shown in Eq. (1), the stress components are composed of two complex functions. Stress components are obtained through the two known complex functions.

Eq. (2) is the relative equation of two stress functions in contact problems [16].

$$\Psi(z) = -\phi(z) - \overline{\phi(\bar{z})} - z\phi'(z) \tag{2}$$

Substituting Eq. (2) for Eq. (1), Eq. (3) is obtained and is expressed by only one stress function $\phi(z)$.

$$\begin{aligned}\sigma_x &= \mathrm{Re}\left[3\phi(z) + \overline{\phi(\bar{z})} + z\phi'(z) - \bar{z}\phi'(z)\right]\\ \sigma_y &= \mathrm{Re}\left[\phi(z) - \overline{\phi(\bar{z})} - z\phi'(z) + \bar{z}\phi'(z)\right]\\ \tau_{xy} &= \mathrm{Im}\left[-\phi(z) - \overline{\phi(\bar{z})} - z\phi'(z) + \bar{z}\phi'(z)\right]\end{aligned} \tag{3}$$

The Muskhelishvili potential $\phi(z)$, that is, the stress function $\phi(z)$, is defined as Eq. (4a) [15].

$$\phi(z) = \frac{1}{2\pi i}\int_{contact}\frac{p(x) - iq(x)}{x - z}dx \tag{4a}$$

$$\phi(z) = \frac{1 - if}{2\pi i}\int_{contact}\frac{p(x)}{x - z}dx \tag{4b}$$

$q(x) = fp(x)$, where $q(x)$ is the frictional force. $\phi(z)$ is expressed by Eq. (4b), f is the frictional coefficient between two contact surfaces. $p(x)$ and $q(x)$ are the pressure distribution function for the contact surface and the distribution function of frictional force, respectively.

$p(x)$ and $q(x)$ are expressed as Eq. (5a) and Eq. (5b), respectively [16].

$$p(x) = -p_0\sqrt{1 - (x/a)^2} \qquad |x| \le a \tag{5a}$$

$$q(x) = -fp_0\sqrt{1 - (x/a)^2} \qquad |x| \le a \tag{5b}$$

where, a is the half length of the contact length, and p_0 is the maximum contact pressure. Contact length a is obtained through experiment. p_0 is calculated by formula. Substitute Eq. (5) for the Muskhelishvili potential ϕ, that is, Eq. (4), and then Eq. (6) is obtained.

$$\phi(z) = -(p_0/2)(i + f)[z - \sqrt{(z^2 - 1)}] \tag{6}$$

Substitute $\phi(z)$, $\phi'(z)$, $\overline{\phi(z)}$ and $\overline{\phi(\bar{z})}$ for Eq.(3) and substituting the position coordinates of the contact line of the contact body for Eq. (3). The contact stresses on the contact line of the contact body are obtained. These processes are called the Hertz's contact theory.

2.2 Photoelastic experimental hybrid method for traction free boundary

As shown in Eq. (1), stress components are composed of stress functions $\phi(z)$ and $\psi(z)$. If two stress functions $\phi(z)$ and $\psi(z)$ are known, the stress components σ_x, σ_y, τ_{xy} can be obtained. Therefore, it is important to know the stress functions $\phi(z)$ and $\psi(z)$. Stress functions $\phi(z)$ and $\psi(z)$ are analytic functions. So they are expressed as power series. If the coefficients of stress functions $\phi(z)$ and $\psi(z)$ are determined, the stress function can be determined; thus, it is most important to obtain the coefficients of the stress function. Using the relative equation of two stress functions and experimental data, the coefficients of the stress function are determined. The rela-

tive equation for the two stress functions is determined from the loading conditions on the boundary of the specimen. To obtain the relative equation for the two stress functions, the conformal mapping function associated with geometrical conditions of the member in the consideration is needed. The conformal mapping function is defined as Eq. (7) as follows:

$$z = \omega(\zeta) \tag{7}$$

$\zeta = \xi + i\eta$ is the complex plane of conformal mapping, and $z = x + iy$ is the complex plane of actual plane.

When an external force is not applied to the surface, σ_y and τ_{xy} are zero on the surface, that is, representing a traction free surface.

Using $\sigma_{yy} - i\tau_{xy}(=\sigma_{rr} - i\tau_{ro}) = 0$ and Eq. (7) and integrating the equation, Eq. (8) is obtained [17].

$$\psi(\zeta) = -\frac{\overline{\omega}(\zeta)}{\omega'(\zeta)}\phi'(\zeta) - \overline{\phi}(\zeta) \tag{8}$$

As stress function $\phi(\zeta)$ is an analytical function, $\phi(\zeta)$ can be expressed by power series.

$$\phi(\zeta) = \sum_{n=0}^{N} C_n \zeta^n = \sum_{n=0}^{N} (a_n + ib_n)\zeta^n \tag{9}$$

$\phi'(z)$, $\psi'(z)$ and $\phi''(z)$ are obtained by using $z = w(\zeta)$, Eq. (8) ,and Eq. (9).Substituting $\phi'(z)$, $\psi'(z)$ and $\phi''(z)$ for Eq. (1), the stress components σ_x, σ_y, τ_{xy} are obtained by Eq. (10)

$$\begin{aligned}\sigma_x &= \mathrm{Re}\left[2\phi'(z) - \overline{z}\phi''(z) - \psi'(z)\right] \\ &= \sum_{n=1}^{N} \mathrm{Re}\left\{C_n\left[2F(n,\zeta) - G(n,\zeta)\right] + \overline{C}_n F(n,\zeta)\right\}\end{aligned} \tag{10a}$$

$$\begin{aligned}\sigma_y &= \mathrm{Re}\left[2\phi'(z) + \overline{z}\phi''(z) + \psi'(z)\right] \\ &= \sum_{n=1}^{N} \mathrm{Re}\left\{C_n\left[2F(n,\zeta) + G(n,\zeta)\right] - \overline{C}_n F(n,\zeta)\right\}\end{aligned} \tag{10b}$$

$$\begin{aligned}\tau_{xy} &= \mathrm{Im}\left[\overline{z}\phi''(z) + \psi'(z)\right] \\ &= \sum_{n=1}^{N} \mathrm{Im}\left\{C_n G(n,\zeta) - \overline{C}_n F(n,\zeta)\right\}\end{aligned} \tag{10c}$$

$$F(n,\zeta) = \frac{n\zeta^{n-1}}{\omega'(\zeta)} \tag{10d}$$

$$\begin{aligned}G(n,\zeta) = &\left[\frac{\overline{\omega}(\overline{\zeta}) - \overline{\omega}(\zeta)}{\omega'^2(\zeta)}\right] n(n-1)\zeta^{n-2} \\ &- \left[\frac{\overline{\omega}(\overline{\zeta}) - \overline{\omega}(\zeta)}{\omega'^3(\zeta)}\omega''(\zeta) + \frac{\overline{\omega}'(\zeta)}{\omega'^2(\zeta)}\right] n\zeta^{n-1}\end{aligned} \tag{10e}$$

$F(n,\zeta)$ and $G(n,\zeta)$ are functions of the position vector determined by using the physical coordinate $z = x + iy$ and the inverse mapping function $\zeta = \omega^{-1}(z)$. Therefore, Eq. (10) is only a function of a_n and b_n. Eq. (11) is the stress optic law for isotropic materials [18].

$$\left(\frac{f_\sigma \cdot N_f}{t}\right)^2 = (\sigma_x - \sigma_y)^2 + (2\tau_{xy})^2 \tag{11a}$$

$$\left(\frac{f_\sigma \cdot N_f}{t}\right)^2 - (\sigma_x - \sigma_y)^2 - (2\tau_{xy})^2 = D(\varepsilon) \tag{11b}$$

f_σ, N_f and t are the stress fringe value, fringe order and thickness of specimen, respectively, and substituting the accurate experimental data for Eq. (11a), Eq. (11a) can not be exactly established. Errors occurred in Eq. (11a), and then $D(\varepsilon)$ can not be zero. To minimize the errors of the given conditions, the numerical method should be used. Substituting Eq. (10) for Eq. (11b), Eq. (12) is obtained.

$$\begin{aligned}D(\varepsilon) &= \left(\frac{f_\sigma \cdot N_f}{t}\right)^2 - (\sigma_x - \sigma_y)^2 - (2\tau_{xy})^2 \\ &= \left(\frac{f_\sigma \cdot N_f}{t}\right)^2 - \left\{\sum_{n=1}^{N} a_n \mathrm{Re}\left[2F(n,z) - 2G(n,z)\right] \right. \\ &\quad \left. + \sum_{n=1}^{N} b_n \mathrm{Im}\left[2F(n,z) + 2G(n,z)\right]\right\}^2 \\ &\quad - \left\{\sum_{n=1}^{N} a_n \mathrm{Im}\left[2G(n,z) - 2F(n,z)\right] \right. \\ &\quad \left. + \sum_{n=1}^{N} b_n \mathrm{Re}\left[2F(n,z) + 2G(n,z)\right]\right\}^2\end{aligned} \tag{12}$$

where $F(n,z)$ and $G(n,z)$ are shown in Eqs. (10d) and (10e), respectively. N_f, t and f_σ are measured by experiment. Therefore Eq. (12) is only a function of $c_n(=a_n + ib_n)$.

Applying Hook and Jeeves' numerical method [19]

to Eq. (12) with experimental data N_f, t, f_σ and position vectors $(z = x + iy)$, c_n is obtained, which is satisfied with the error limit. Substituting c_n for Eq. (9) and for Eq. (8), stress functions $\phi(z)$ and $\psi(z)$ are obtained. Substituting the obtained $\phi(z)$ and $\psi(z)$ for Eq. (1), σ_x, σ_y and τ_{xy} are determined, which are in the structures under arbitrary loads.

These procedures are called the photoelastic experimental hybrid method, that is, hybrid method I. The traditional free boundary condition is comprised of the internal traction free boundary condition and the external traction free boundary condition. Until now, the photoelastic experimental hybrid method has been applied to internal traction free boundary condition problems such as circular hole and crack problems.

2.3 Photoelastic experimental hybrid method for O-ring under uniform squeeze

Fig. 1 shows restraint conditions of the O-ring under uniform squeeze. Squeeze rate is defined as $x/d \times 100$, when x is compressive deformation of O-ring diameter (=d) due to contact force.

When it is under uniform squeeze, the O-ring can be changed into the configuration of Fig. 2. Eq. (13) is the mapping function of region R in Fig. 2. Region R_ζ in the conformal mapping plane is defined by $z = \omega(\zeta) = (1-\xi)/(1+\xi)$ [20].

$$z = \omega(\zeta) = \frac{i-\zeta}{i+\zeta} \tag{13}$$

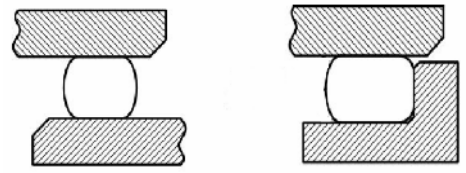

(a) Uniform squeeze (b) Uniform squeeze with one-side lateral restrain

Fig. 1. Restraint conditions of O-ring under squeeze.

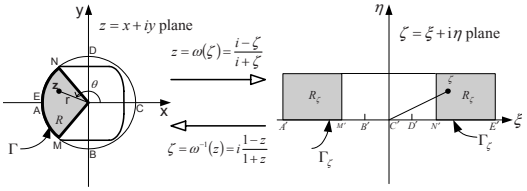

Fig. 2. Conformal mapping for O-ring under uniform squeeze.

Substituting $\overline{\omega}(\zeta)$, $\overline{\omega}(\overline{\zeta})$, $\omega'(\zeta)$, $\overline{\omega}'(\zeta)$, $\omega'^2(\zeta)$, $\omega'^3(\zeta)$, $\omega''(\zeta)$ for Eq.(10d) and Eq. (10e), $F(n,z)$ and $G(n,z)$ are obtained as follows.

$$F(n,z) = -2ni\frac{(i-z)^{n-1}}{(i+z)^{n+1}}$$

$$G(n,z) = -4n(n-1)(z+\overline{z})\frac{(i-z)^{n-2}}{(i+z)^{n+2}} + \left[4i(z+\overline{z}) + 2(i+z)\right]n\frac{(i-z)^{n-1}}{(i+z)^{n+2}} \tag{14}$$

When fringe orders and the position coordinates associated the fringe order in isochromatic fringe patterns of O-ring are measured and repeat numbers are given, $F(n,z)$ and $G(n,z)$ are determined. Eq. (12) is only a function of a_n and b_n. Applying the Hook and Jeeves' numerical method to Eq. (12) with the experimental data of the O-ring, a_n and b_n are determined. And then, stress functions $\phi(z)$ and $\psi(z)$ are determined. Stress components in the O-ring are determined.

Applying the photoelastic experimental hybrid method to structures such as an O-ring, that is, a member with external traction free boundary condition, stress components are obtained.

In contact problems, there is another photoelastic experimental hybrid method. In the photoelastic experimental hybrid method, it is most important to establish the relative equation of two stress functions.

In a contact problem, Eq. (2) is the relative equation of both stress functions

Eq. (2) can be used instead of Eq. (8).

Both stress functions $\phi(z)$ and $\psi(z)$ are analytical functions, and therefore, they can be expressed by power series as Eq. (15)

$$\phi(z) = \sum_{n=0}^{N} C_n z^{\frac{n}{2}} \tag{15a}$$

$$\psi(z) = \sum_{n=0}^{N} D_n z^{\frac{n}{2}} \tag{15b}$$

Substitute Eq. (15a) and Eq. (15b) for Eq. (2). The relative equation of the complex coefficients in both stress functions is obtained by Eq. (16)

$$D_n = -\frac{n}{2}C_n - \overline{C_n} \tag{16}$$

Substituting both stress functions using Eq. (16) for Eq. (1), Eq. (17) is obtained.

$$\sigma_x(z)=\sum_{n=1}^{N}\mathrm{Re}\left\{C_n\left[2F(n,z)-G(n,z)\right]+\bar{C}_nF(n,z)\right\}$$

$$\sigma_y(z)=\sum_{n=1}^{N}\mathrm{Re}\left\{C_n\left[2F(n,z)+G(n,z)\right]-\bar{C}_nF(n,z)\right\}$$

$$\tau_{xy}(z)=\sum_{n=1}^{N}\mathrm{Im}\left\{C_nG(n,z)-\bar{C}_nF(n,z)\right\} \qquad (17)$$

where $F(n,z)=\frac{n}{2}z^{\frac{n}{2}-1}$,

$$G(n,z)=\frac{n}{2}\left[\left(\frac{n}{2}-1\right)\bar{z}-\frac{n}{2}z\right]z^{\frac{n}{2}-2}$$

The remaining procedures are the same as the photoelastic experimental hybrid method explained above. These processes are called hybrid method II.

3. Experiment and experimental method

3.1. Specimen

To study the contact stress of the O-ring by using the photoelastic experiment, a model of an O-ring was made of polymer, which has photoelastic properties.

In this research, epoxy resin was used as model material. The cross-sectional diameter of the O-ring is $6.98\pm0.15mm$, and the internal diameter of the O-ring is $121.5\pm0.94mm$.

The photoelastic material used in this research was epoxy resin, which is made from Araldite and hardener (Ciba-Geigy Co., weight ratio : 10:3).

Molding procedures of the O-ring are as follows

(1) Make steel into an O-ring, which is identical to the O-ring of this study.

(2) Make a molding box and put the steel O-ring in the box.

(3) Pour silicon into the molding box and take out the steel O-ring from the silicon block after 12 hours. Then, the molding box for O-ring has been made.

(4) Measure the Araldite and hardener(weight ratio : 10:3), put them into the separating vessel and heat them for 2 hours at 130℃ in the stress freezing furnace. Then they are changed into liquid.

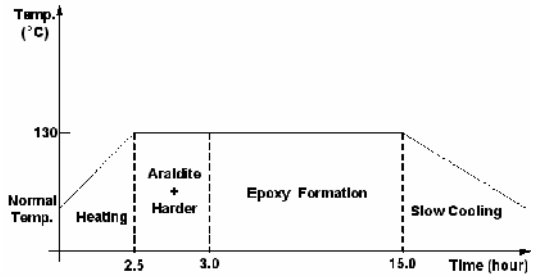

Fig. 3. Molding cycle in furnace.

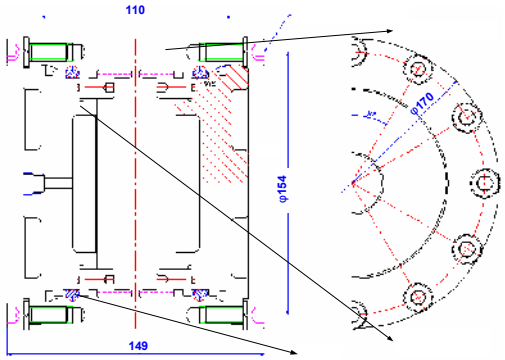

Fig. 4. Loading device for O-ring under uniform squeeze rate.

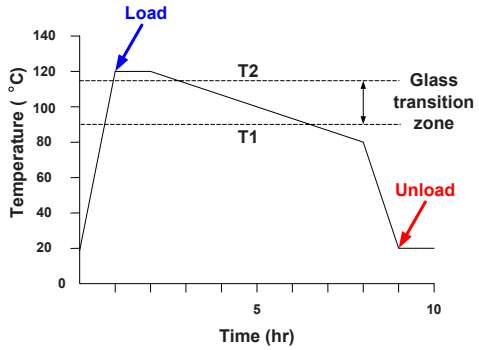

Fig. 5. Stress freezing cycle for epoxy resin.

(5) Pour hardener into the dissolved Araldite and mix them two or three times at an interval of 5 minutes. Push the mixed epoxy resin into the molding box using an injector and completely remove the bubbles in the mixed epoxy resin.

(6) Heat molding box and cool down according to molding cycle, as shown in Fig. 3

(7) Take the O-ring made from the epoxy resin out from molding box.

3.2. Loading device and isochromatic fringe pattern

Fig. 4 shows the experimental loading device which

uniform squeeze can be applied, squeeze rate was controlled by internal diameter variations of the groove. The O-ring made from epoxy resin, cylinder , and guide-ring were heated for 40 minutes at 120℃ in the furnace. The O-ring, cylinder and guide-ring were assembled in the furnace. The assembled loading device was heated according to the stress freezing cycle, as shown in Fig. 5 , in the furnace.

The O-ring with freezing stress was cut at 90° intervals. Slices were cut by 2mm. They were ground until their thickness was about 1mm. The finished slices were put into the box with a mixed solution of α-bromnaphtalene and fluid parapin at 1:0.585 volume ratio. The glass box with the finished slices was put on the loading position of the transparent photoelastic experimental device. Isochromatic fringe patterns were recorded in the file with a digital camera.

3.3 Photoelastic experimental hybrid method for stress analysis of O-ring

Processes of photoelastic experimental hybrid method for stress analysis of O-ring are as follows.

1. Measure the mechanical properties of elastic modulus ($= E : 15.6MPa$) , Poisson's ratio ($= v : 0.5$) and stress fringe values ($= f_\sigma : 4.12m/kN$) .

2. Magnify the isochromatic fringe patterns of each slice and record them in the personal computer through a digital camera.

3. Measure 150~200 experimental data and 350-400 experimental data on the fringe orders of 0.5 times for squeeze rates of 10% and 20%, respectively.

4. Substitute the measured experimental data for the stress optic law and apply the Hook and Jeeves' numerical method to the stress optic law with experimental data.

C_n is calculated. when C_n is determined, $F(n,z)$ and $G(n,z)$ should be used in accordance with the procedures of the photoelastic experimental hybrid method.

A stress function is obtained and another stress function is obtained from the relative equation of two stress functions. Stress components are obtained by using Eq. (1) and two stress functions.

5. Substitute the stress components obtained above for the stress optic law and plot the isochromatic fringe pattern. Compare the actual isochromatic fringe pattern with the graphing isochromatic fringe pattern.

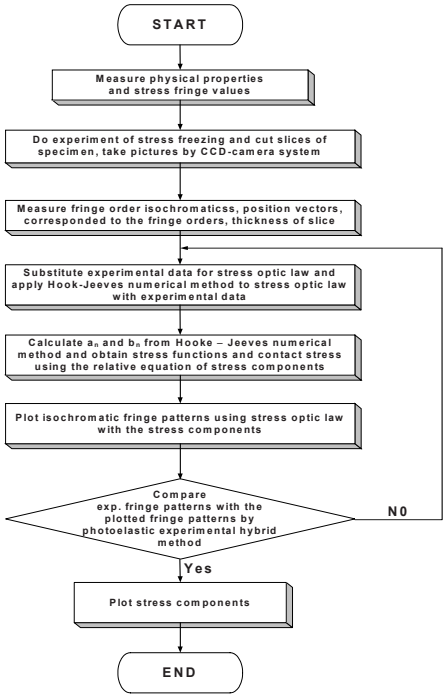

Fig. 6. Flow chart of photoelastic experimental hybrid method for the contact problem of O-ring under uni-form squeeze rate.

If the graphing isochromatic fringe pattern is identical to the actual isochromatic fringe pattern, go to the next procedure. If the graphing isochromatic fringe pattern is not identical to the actual isochromatic fringe pattern, repeat the above processes until the graphing isochromatic fringe pattern is almost identical to the actual isochromatic fringe pattern.

6. When the graphing isochromatic fringe pattern is identical to the actual isochromatic fringe pattern, stress functions are determined. Contact stresses and internal stresses of the O-ring are determined. Plot the stress contour of the stress components normalized by the maximum contact pressure.

Fig. 6 shows the flow chart of the photoelastic experimental hybrid method for the contact problem of the O-ring under uniform squeeze rate.

4. Experimental results and discussions

Isochromatic fringe patterns of position 1, position 2, position 3, and position 4 are identical to each other for squeeze rates of 10% and 20%, each position is located along O-ring by 90° internal. Therefore, in this research, the isochromatic fringe patterns of posi-

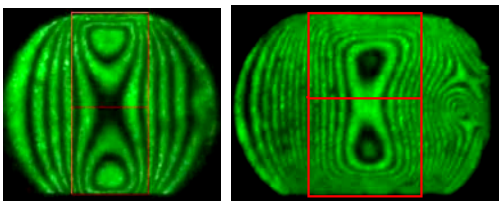

(a) Position1(10%) (b) Position1(20%)

Fig. 7. Isochromatic fringe patterns of position 1 in O-ring under uniform squeeze rate.

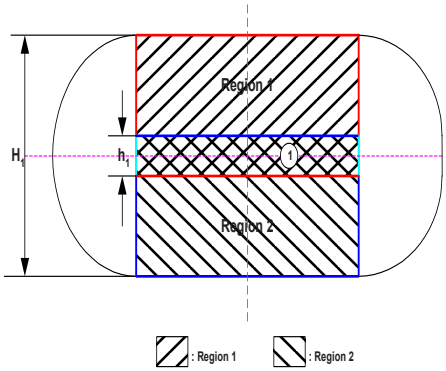

Fig. 8. Measured regions of photoelastic isochromatic data in the deformed O-ring.

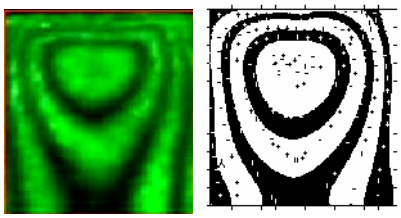

(a) Region 1 of position 1

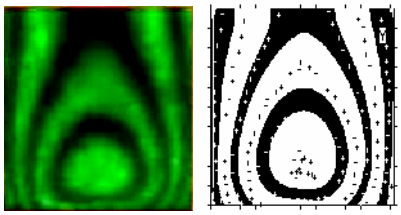

(b) Region 2 of position 1

Fig. 9. Actual isochromatic fringe pattern of position 1(left side) and graphic isochromatic fringe pattern of position 1 obtained from the photoelastic experimental hybrid method(right side)(squeeze rate : 10%).

tion 1 are introduced. Fig. (a) and Fig. (b) in Fig. 7 show the isochromatic fringe patterns of position 1 for squeeze rates of 10% and 20%.

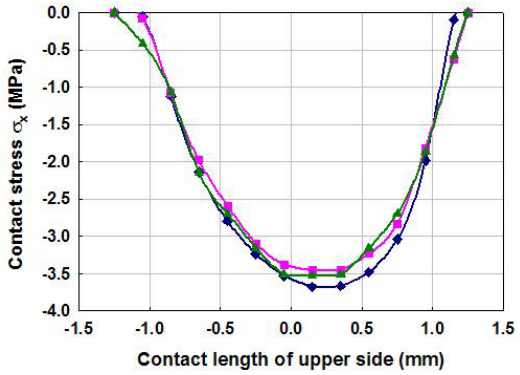

Fig. 10. Distributions of contact stress σ_x of upper side of O-ring under 10% squeeze rate.

Fig. 8 shows the measured regions of the photoe lastic isochromatic data. The measured data in region 1 and region 2 were the used to obtain stress components in region 1 and region 2. The isochromatic fringe patterns of each position were identical to each other, and the isochromatic fringe pattern of position 1 was used to obtain the stress components.

Fig. (a) and Fig. (b) in Fig. 9 show actual isochromatic fringe pattern(left-side) and graphic isochromatic fringe pattern(right side)of region 1 and region 2 of position 1, respectively. "+" symbol indicates the position at which the fringe orders were measured. All "+" symbols were almost located on the centerline of the black or white band.

The graphic isochromatic fringe pattern was almost identical to the actual isochromatic fringe pattern.

Therefore, the above results show that the photoelastic experimental hybrid method for the contact problems of both cylinders was effective.

In Fig. 10, Fig. 11, Fig. 12, Fig. 17, Fig. 18, and Fig. 19, the diamond(—◆—) indicates stress components of the contact stress obtained from the Hertz's contact theory. The square (—■—) and triangle(—▲—) indicate stress components of the contact stresses obtained from hybrid method I and hybrid method II respectively. Fig. 10 shows the contact stress distributions σ_x of the upper side of O-ring under 10% squeeze rate. As shown in Fig. 10, the contact stress distribution of σ_x are almost identical to each other. The center of the distributions of σ_x is moved slightly to the right from the center of the contact length.

These situations occurred due to the frictional force between the O-ring and cylinder when the O-ring and

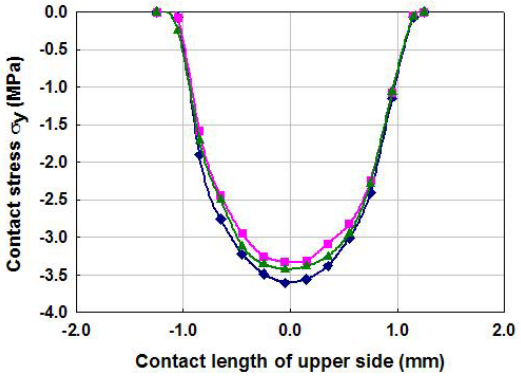

Fig. 11. Distributions of contact stress σ_y of upper side of O-ring under 10% squeeze rate.

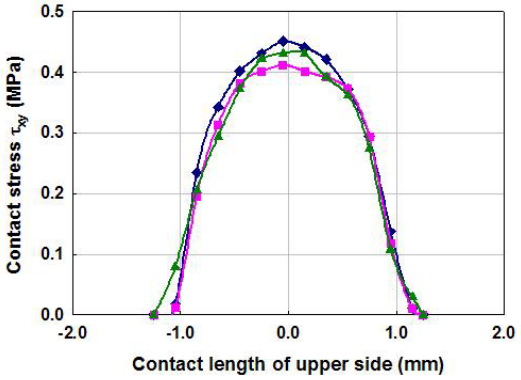

Fig. 12. Distributions of contact stress τ_{xy} of upper side of O-ring under 10% squeeze rate.

cylinder were assembled. The maximums of σ_x obtained from the Hertz contact theory, hybrid method Ⅰand hybrid method Ⅱwere -3.675Mpa, -3.459MPa and -3.528MPa , respectively. The contact length of the O-ring was 2.502 mm.

Fig. 11 shows the contact stress distributions σ_y of the upper side of the O-ring under 10% squeeze rate. As shown in Fig. 11, the stress components σ_y obtained from the Hertz's contact theory, hybrid method Ⅰ and hybrid method Ⅱ are almost identical to each other. Stress distributions of σ_y are almost symmetrical about the center of contact length. The maximums of absolute σ_y obtained from the Hertz's theory, hybrid method Ⅰ and hybrid method Ⅱare -3.606MPa, -3.332MPa and -3.430MPa , respectively.

Fig. 12 shows contact stress distributions τ_{xy} of the upper side of the O-ring under 10% squeeze rate. Stress distributions of τ_{xy} obtained from Hertz the ory, hybrid method Ⅰ and hybrid method Ⅱ are almost identical to each other. They are almost symmetrical about the center of the contact length. The maximums of τ_{xy} obtained from the Hertz theory, hybrid method Ⅰ and hybrid method Ⅱ are 0.451MPa, 0.412MPa and 0.431MPa , respectively.

Stress distributions of the lower side are almost identical to those of the upper side. The maximum of absolute σ_x in the upper side or lower side is slightly greater than the maximum of the absolute σ_y in the upper side or lower side. Their values are almost identical to each other. These effects occurred due to the frictional force between the O-ring and cylinder.

As shown in Figs. 10, 11 and 12, the maximum of absolute σ_x occurs at a point moved from the center of the contact length by 0.25mm. The maximums of absolute σ_y and τ_{xy} occur at the center of the contact length. Stress components σ_x, σ_y and τ_{xy} in the upper side are slightly greater than those in the lower side . τ_{xy} is 1/8 of σ_x or σ_y. These situations occur because the upper side of O-ring contacts in advance than the lower side of O-ring.

Fig. (a), (b) and (c) in Fig. 13 show the stress contours of σ_x/p_0 obtained from the Hertz theory, hybrid method Ⅰ and hybrid method Ⅱ in region 1 and in region 2 of the O-ring under 10% squeeze rate , respectively. Stress contours of the internal stress σ_x/p_0 are the stress components σ_x normalized by the maximum contact pressure p_0 in region 1 and region 2.

They are expressed in 0.1unit. a is half of the contact length measured by experiment. p_0 is obtained by using a formula [16] and half of the contact length $(=a)$.

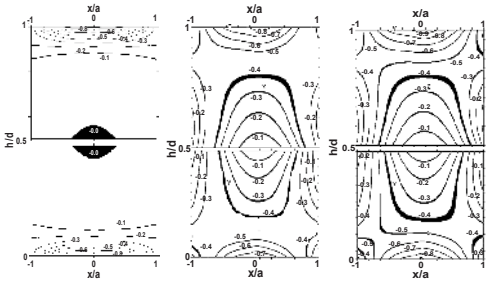

(a) Hertz theory (b) Hybrid Ⅰ (c) Hybrid Ⅱ

Fig. 13. Stress contours of internal stress σ_x/p_0 obtained from the Hertz theory, hybrid method Ⅰ and hybrid method Ⅱ in region 1 and in region 2 of O-ring under 10% squeeze rate.

Stress distributions of Fig. (b) in Fig. 13 are almost similar to those of Fig. (c) in Fig.13. The maximum of the absolute internal stress σ_x/p_0 obtained from hybrid method Ⅱ is greater than that of the absolute internal stress σ_x/p_0 obtained from hybrid method Ⅰ by 0.1.

Continuity of the stress contours in region 1 and region 2 was very good. But the stress contours in region 1 were not completely connected to those in region 2.

When the squeeze rate was 10%, the distributions and shapes of σ_x/p_0 obtained from hybrid method Ⅰ were similar to those from hybrid method Ⅱ. The maximums of the absolute internal stress σ_x/p_0 obtained from Hertz theory, hybrid method Ⅰ and hybrid method Ⅱ occurred at the center of the contact length.

Their maximum values of the absolute internal stress σ_x/p_0 were 0.8, 0.8 and 0.9.

Fig. (a), (b), and (c) in Fig.14 show stress contours of internal stress σ_y/p_0 obtained from the Hertz theory, hybrid method Ⅰ and hybrid method Ⅱ, respectively , in region 1 and region 2 of the O-ring under 10% squeeze rate

The stress contours of internal stress σ_y/p_0 are the stress components of the internal stress σ_y normalized by the maximum contact pressure p_0 in region 1 and region 2. They are expressed in 0.1unit. Distributions of σ_y/p_0 stress contours of the internal stress obtained from the Hertz theory were different from those obtained from hybrid method Ⅰ and hybrid method Ⅱ.

But the distributions of σ_y/p_0 stress contours of the internal stress obtained from hybrid method Ⅰ were similar to those obtained from hybrid method Ⅱ.

As shown in Fig.14, in all cases, the maximums of the absolute internal stresses σ_y/p_0 occur at the center of the contact length. Their values are 0.9, 1.0 and 1.0 , respectively.

The maximum of absolute σ_y/p_0 obtained from hybrid method Ⅰ occurs at $x/a=-0.1$ in region 1 or region 2.

The centers of another absolute internal stress σ_y/p_0 obtained from hybrid method Ⅰ except for the maximum of absolute σ_y/p_0 are located at $x/a=0$ in region 1. But they are located at an arbitrary point in region 2.

All maximums of absolute internal stresses σ_y/p_0 obtained from hybrid method are almost at the center

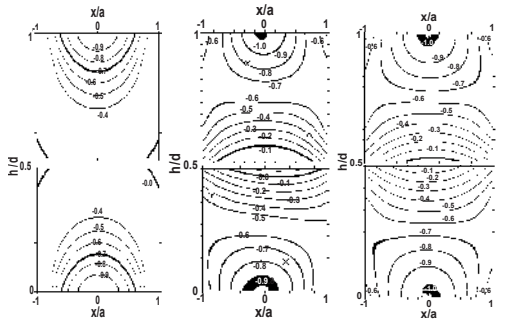

(a) Hertz theory (b) Hybrid Ⅰ (c) Hybrid Ⅱ

Fig. 14. Stress contours of internal stress σ_y/p_0 obtained from the Hertz theory, hybrid method Ⅰ and hybrid method Ⅱ in region 1 and region 2 of O-ring under 10% squeeze rate.

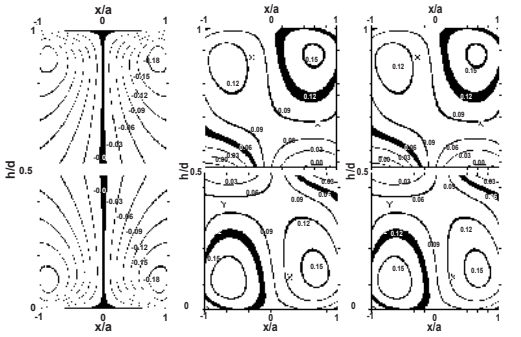

(a) Hertz theory (b) Hybrid Ⅰ (c) Hybrid Ⅱ

Fig. 15. Stress contours of internal stress τ_{xy}/p_0 obtained from the Hertz theory, Hybrid method Ⅰ and Hybrid method Ⅱ.

of the contact length. Maximum value of absolute internal stress σ_y/p_0 is 1.0.

Fig. (a), Fig. (b) and Fig. (c) in Fig. 15 show internal stress τ_{xy} normalized by p_0 in region 1 and in region 2 of O-ring under 10% squeeze rate, respectively. They are internal stresses τ_{xy}/p_0 obtained from Hertz theory, hybrid method Ⅰ and hybrid method Ⅱ, respectively.

They are smaller than the other stress components, that is, internal stresses σ_x/p_0 and internal stresses σ_y/p_0 .

The stress distributions obtained from Hertz theory are symmetrical on the right side and on left side about $x/a=0$ in upper side and in lower side about $h/d=0.5$.

Stress distributions obtained from hybrid method Ⅰ are very similar to those from hybrid method Ⅱ in region 1 and in region 2.

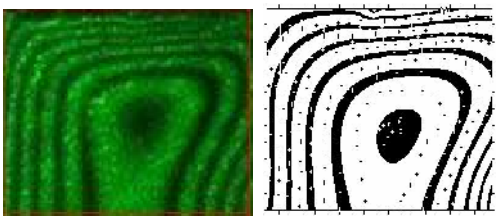

(a) Region of position 1

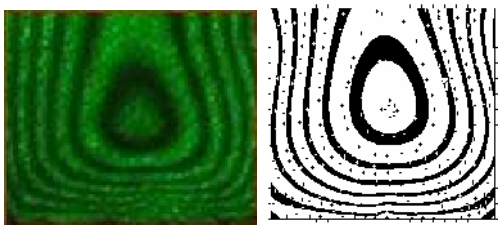

(b) Region of position 2

Fig. 16. Actual photoelastic fringe patterns(left side) of position 1 and graphic photoelastic fringe patterns from the photoelastic experimental hybrid method(right side) (squeeze rate : 20%).

Fig. (a) and Fig. (b) in Fig. 16 show actual photoelastic fringe patterns(left side) and graphic photoelastic fringe patterns(right side) obtained from the photoelastic experimental hybrid method in region 1 and region 2 ,respectively, when squeeze rate of O-ring is 20%.

In graphic photoelastic fringe patterns, all "+" symbols indicate the positions at which the fringe orders were measured. They were measured on the center line of each black and white band. The graphic photoelastic fringe patterns are almost indentical to the actual photoelastic fringe patterns. All "+" symbols are located on the center line of each black and white band. The results mean that the photoelastic experimental hybrid method was effective on the stress analysis problems of the O-ring under uniform squeeze rate.

Fig. 17 shows contact stress distributions σ_x of the upper side of the O-ring under 20% squeeze rate. In Fig. 17(Fig. 18 and Fig. 19), diamond( ), square( ), and triangle( ) symbols indicate the contact stress $\sigma_x(\sigma_y, \tau_{xy})$ obtained from the Hertz theory, Hybrid method Ⅰ and Hybrid method Ⅱ, respectively.

As shown in Fig. 17, they are almost identical to each other. The maximum of absolute σ_x obtained from hybrid method Ⅱ is almost identical to the maximum of absolute σ_x obtained from Hybrid Ⅰ.

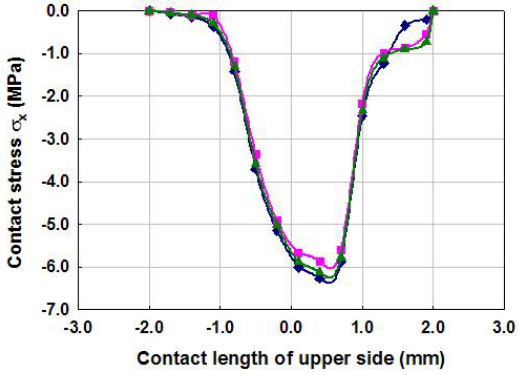

Fig. 17. Distributions of contact stress σ_x of upper side of O-ring under 20% squeeze rate.

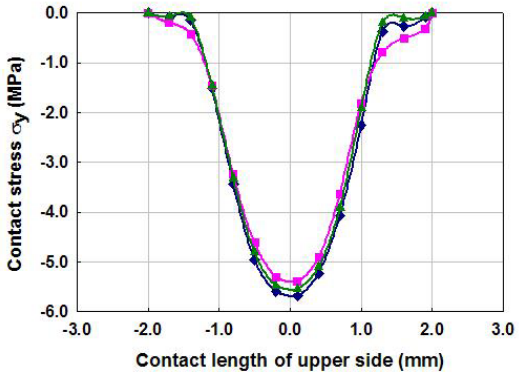

Fig. 18. Distributions of contact stress σ_y of upper side of O-ring under 20% squeeze rate.

Values of σ_x obtained from Hertz theory, hybrid method Ⅰ and hybrid method Ⅱ are -6.202MPa, -5.870MPa and -6.125MPa, respectively.

The maximums of σ_x are moved slightly to the right side from the center of the contact length. The O-ring is in close contact with the right side of the groove due to the frictional force between the cylinder and the O-ring when the O-ring and cylinder were assembled.

Fig. 18 shows the contact stress distributions σ_y of the upper side of the O-ring under 20% squeeze rate. Distributions of contact stresses σ_y obtained from Hertz theory, hybrid method Ⅰ and hybrid method Ⅱ are identical to each other. Their distributions are symmetrical about the center of the contact length. The values of σ_y obtained from Hertz theory, hybrid method Ⅰ and hybrid method Ⅱ are -5.684 MPa, -5.547 MPa and -5.390 MPa , respectively.

Fig. 19 shows the contact stress distributions τ_{xy} of the upper side of the O-ring under 20% squeeze

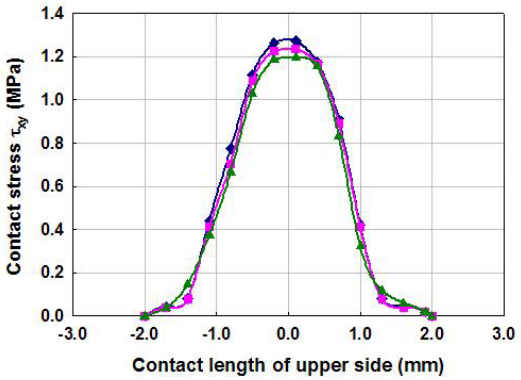

Fig. 19. Distributions of contact stress τ_{xy} of upper side of O-ring under 20% squeeze rate.

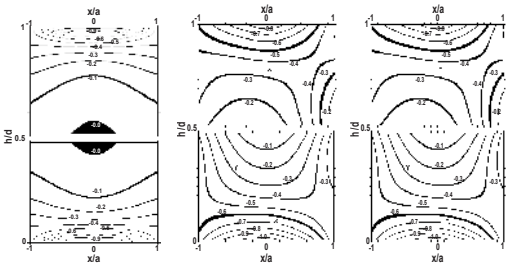

(a) Hertz theory (b) Hybrid Ⅰ (c) Hybrid Ⅱ

Fig. 20. Internal stress contours of σ_x/p_0 obtained from Hertz theory, hybrid method Ⅰ and hybrid method Ⅱ for O-ring under 20% squeeze rate.

rate. Stress distributions τ_{xy} obtained from the Hertz theory, hybrid method Ⅰ and hybrid method Ⅱ are almost identical to each other and they are almost symmetrical about the center of contact length. Their maximum values are 1.247MPa, 1.235MPa and 1.196MPa, respectively. Stress distributions of σ_x, σ_y and τ_{xy} of the lower side of the O-ring are very similar to those of the upper side of the O-ring. The maximums of absolute σ_x in the lower side and in the upper side of O-ring are greater than maximum of σ_y on the lower side and on the upper side of the O-ring, respectively, under 20% squeeze rate. But their values are almost equal to each other. The maximums of absolute σ_x occur at a point slightly moved from the center of the contact length. The maximums of absolute σ_y and τ_{xy} occur at the center of the contact length. These situations were resulted from the frictional force between the O-ring and the cylinder. The maximums of τ_{xy} are about 1/5 of the maximums of absolute σ_x and absolute σ_y. Stress components absolute σ_x, absolute σ_y and τ_{xy} of the upper side of the O-ring are greater than those of

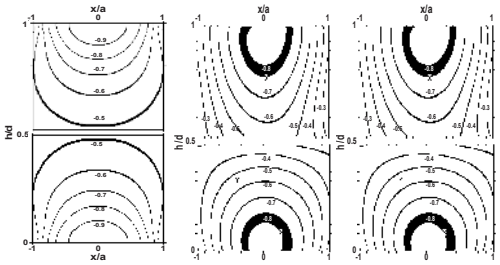

(a) Hertz theory (b) Hybrid Ⅰ (c) Hybrid Ⅱ

Fig. 21. Internal stress contours of σ_y/p_0 obtained from the Hertz theory, hybrid method Ⅰ and hybrid method Ⅱ for O-ring under 20% squeeze rate.

the lowerside of the O-ring under 20% uniform squeeze rate.

Fig. (a), Fig. (b) and Fig. (c) in Fig.20 show the internal stress distributions of σ_x/p_0 normalized by maximum contact pressure p_0 in region 1 and region 2, of the O-ring under uniform 20% squeeze rate. They are obtained from Hertz theory, hybrid method Ⅰ and hybrid method Ⅱ, respectively. They are represented in 0.1 unit. Internal stress distribution patterns of σ_x/p_0 obtained from Hertz theory, hybrid method Ⅰ and hybrid method Ⅱ are different from each other. But internal stress magnitudes of σ_x/p_0 obtained from Hertz theory, hybrid method Ⅰ and Hybrid method Ⅱ are similar to each other. There are some differences between their maximums. The internal stress contours of σ_x/p_0 obtained from hybrid method Ⅰ and hybrid method Ⅱ on the upper side of the O-ring are smoothly connected to those on the lower side of the O-ring than those from the Hertz theory on the lower side of the O-ring. The maximum of the internal stresses σ_x/p_0 obtained from hybrid method Ⅱ is greater than that obtained from hybrid method Ⅰ by 0.2 in the upper side of the O-ring. The maximums of the internal stresses σ_x/p_0 obtained from Hertz theory, hybrid method Ⅰ and hybrid method Ⅱ are 0.9, 0.8 and 1.0, respectively. They occur at the center of the contact length in the O-ring under 20% squeeze rate.

Fig. (a), Fig. (b) and Fig. (c) in Fig. 21 show the internal stress contours of σ_y/p_0 obtained from the Hertz theory, hybrid method Ⅰ and hybrid method Ⅱ for the O-ring under 20% squeeze rate, respectively.

In Fig. (a) of Fig. 21, the maximums of absolute internal stresses σ_y/p_0 occur at the center of the contact line. The maximums of the absolute internal stresses σ_y/p_0 in region 1 and region 2 are 0.9 and

0.9, respectively.

Stress contours obtained from hybrid method Ⅰ and hybrid method Ⅱ are more smoothly connected to those in region 1 and in region 2. All absolute maximums of the internal stress contours σ_y/p_0 obtained from hybrid method Ⅱ occur at the center of the contact line. But maximums of internal stress contours σ_y/p_0 obtained from hybrid method Ⅰ occur at an arbitrary point of the contact line. But they occur in the vicinity of $x/a=0$. The maximums of absolute internal stresses σ_y/p_0 obtained from Hertz theory, hybrid method Ⅰ and hybrid method Ⅱ are 0.9, 0.8 and 0.8 respectively. The maximums of absolute σ_y/p_0 obtained from Hertz theory and hybrid method Ⅱ occur at $x/a=0$. The maximums of absolute σ_y/p_0 obtained from hybrid method Ⅰ in region 1 and region 2 occur at $x/a=-0.1$.

Fig. (a), Fig. (b) and Fig. (c) in Fig.22 show the internal stress contours of τ_{xy}/p_0 obtained from the Hertz theory, hybrid method Ⅰ and hybrid method Ⅱ for the O-ring under 20% squeeze rate, respectively.

The internal stress contours of τ_{xy}/p_0 obtained from the Hertz theory and hybrid method Ⅱ in region 1 are smoothly connected to those in region 2. The distributions of internal stress contours τ_{xy}/p_0 obtained from the Hertz theory and hybrid method Ⅱ in region 1 are almost identical to those in region 2. The continuities of the internal stress contours τ_{xy}/p_0 obtained from the Hertz theory and hybrid method Ⅱ are in good agreement with the stress contours of region 1 and region 2.

The maximums of the stress contour obtained from Hertz theory and hybrid method Ⅱ in region 1 and in region 2 are equal to each other.

The continuity of the internal stress contours τ_{xy}/p_0 obtained from hybrid method Ⅰ is not good agreement with the stress contours in region 1 and region 2. The maximums of the internal stress contour τ_{xy}/p_0 obtained from hybrid method Ⅰ in region 1 are not equal to the maximum of the internal stress contour τ_{xy}/p_0 in region 2. The maximum of τ_{xy} is 1/5 of the maximum of absolute σ_x or maximum of absolute σ_y .The following conclusions were obtained through the above experiments and discussions.

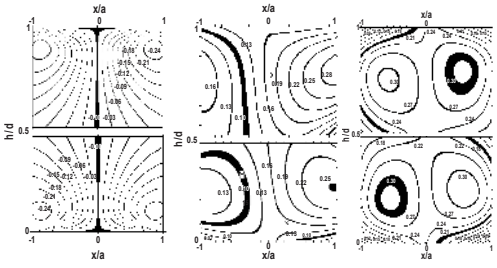

(a) Hertz theory (b) Hybrid Ⅰ (c) hybrid Ⅱ

Fig. 22. Internal stress contours of τ_{xy}/p_0 obtained from the Hertz theory, hybrid method Ⅰ and hybrid method Ⅱ for O-ring under 20% squeeze rate.

5. Conclusions

(1) A photoelastic experimental hybrid method using external traction free boundary condition was developed and its validity was confirmed. It can be effectively used to analyze the contact stress and the internal stresses of a contact body.

(2) A photoelastic experimental hybrid method using the relative equation of two stress functions in a contact problem was developed, and its validity was confirmed. It can be effectively used to analyze the contact stresses and the internal stresses of the contact body.

(3) In the stress analysis of a contact problem, the Hertz theory, the photoelastic experimental hybrid method using external traction free boundary condition (hybrid method Ⅰ) and the photoelastic experimental hybrid method using the relative equation of two stress functions (hybrid method Ⅱ) were used. Among them, the photoelastic experimental hybrid method using the relative equation of two stress functions in the contact problem gave the best results.

(4) With respect to the contact stress of the O-ring under 10% or 20% squeeze rate, the maximum of absolute σ_x was slightly greater than maximum of absolute σ_y; that is, σ_x is almost equal to σ_y. The maximums of absolutes σ_x, σ_y, τ_{xy} on the upper side of the O-ring were greater than those on the lower side of the O-ring by little, respectively. When the squeeze rate of the O-ring was 10%, the maximum of τ_{xy} was 1/8 of the maximum of absolute σ_x or the maximum of absolute σ_y. When the squeeze rate of the O-ring was 20%, the maximum of τ_{xy} was 1/5 of the maximum of absolute σ_x or the maximum of absolute σ_y.

Acknowledgment

This research was supported by Yeungnam university research grant in 2007, Korea.

References

[1] Antonio Strozzi, Static stresses in an unpressurized, rounded, rectangular, elastometric seal, Asle Transactions, 29(4)(1986) 558-564.

[2] E. Dragoni and A. Strozzi, Theoretical analysis of an unpressurized elastomeric O-ring seal into a rectangular groove, Elsevier Sequoia, Wear, 130 (1989) 41-51.

[3] E. Dragoni and A. Strozzi, Analysis of an unpressurized, laterally restrained, elastomeric O-ring seal, Journal of Tribology, 110(1988) 192-300.

[4] A. Karaszkiewicz, Geometry and contact pressure of an O-ring mounted in a seal groove, Ind. Eng. Chem. Res. 29(1990) 2134-2137.

[5] I. K. Lee and C. K. Kim, Numerical simulations on the O-ring extrusion in automotive engines, Journal of Korean Society of Tribologists & Lubrication Engineers, 15(4)(1999) 297-303.

[6] K. K. Chandrashekhara and K. Jacob, Experimental numerical hybrid technique for stress analysis of orthotropic composites, Edited by Holester, Applied Science Publication, (1977) 67-68.

[7] C. W. Smith, D. Post, G. Hiatt and G. Nicoletto, Displacement measurements around cracks in three dimensional Problems by a hybrid experimental technique, Exp. Mech., (1983)15-20.

[8] J. S. Hawong, C. H. Lin, S. T. Lin, J. Rhee and R. E. Rowlands, A hybrid method to determine individual stresses in orthotropic composites using only measured isochromatic data, Journal of Composite Material, 29(18)(1995) 2366-2387.

[9] J. S. Hawong, D. C. Shin and H. J. Lee, Photoelastic experimental hybrid method for fracture mechanics of anisotropic materials, Experimental Mechanics, 41(1)(2001) 92-99.

[10] D. C. Shin, J. S. Hawong, J. H. Nam, H. J. Lee and O. S. Kwon, Application of transparent photoelastic experimental hybrid method for the fracture mechanics of orthotropic material, Transactions of the Korean Society of Mechanical Engineers(A), 22 (6) (1998) 1036-1044.

[11] D. C. Shin, J. S. Hawong, H. J. Lee, J. H. Nam and O. S. Kwon, Application of transparent photoelastic experimental hybrid method to the fracture mechanics of isotropic material, Transactions of the Korean Society of Mechanical Engineers(A), 22 (5) (1998) 834-842.

[12] D. C. Shin and J. S. Hawong, A study on the development of the dynamic photoelastic experimental hybrid method for isotropic material, Transaction of the Korean Society of Mechanical Engineers (A), 24 (9) (2000) 2220-2227.

[13] D. C. Shin and J. S. Hawong, A study on the development of the dynamic photoelastic experimental hybrid method for dissimilar isotropic material, Transactions of the Korean Society of Mechanical Engineers (A), 25 (3) (2001) 434-442.

[14] D. C. Shin, J. S. Hawong and J. H. Sung, Development of the dynamic photoelastic experimental hybrid method for propagating cracks in orthotropic material, Transactions of the Korean Society of Mechanical Engineers (A), 27 (8) (2003) 1273-1280.

[15] N. I. Muskhelishvili, Some basic problems of mathematical theory of elasticity, 4th Edition, P. Noordhoff Ltd., Groningen Netherlands, (1963).

[16] D. A. Hills, D. Nowell and A. Sackfield, Mechanics of elastic contacts, Butterworth-Heinemann, U.S.A. (1993).

[17] Y. –M. Huang, Determination of individual stresses from thermoelastically measured trace of stress tensor, Dissertation, University of Wisconsin-Madison, U.S.A. (1989).

[18] R. C. Sampson, A Stress-optic law for photoelastic analysis of orthotropic composites, Exp. Mech. 10 (1970) 210-215.

[19] M. S. Bazaraa and C. M. Shetty, Nonlinear programming theory and algorithms, John Wiley & Sons Inc. U.S.A. (1979).

[20] Ruel V. Churchill, James W. Brown, Roger F. Verhey., Complex variables and applications, Third Edition, U.S.A. (1974).

Jai-Sug Hawong received a B.S. degree in Mechanical Engineering from Yeungnam Uni-versity in 1974. Then he received his M.S. degree and Ph.D. degree from Yeungnam University in Korea in 1976 and from Kanto Gakuin University in Japan in 1990, respectively. Prof. Hawong is currently a professor at the school of Mechanical Engineering at Yeungnam University, in Gyeongsan city, Korea. He is currently serving as an vise-president of Korea Society Mechanical Engineering. Prof. Hawong's research interests are the areas of static and dynamic fracture mechanics, stress analysis, experimental mechanics for stress analysis and composite material etc.